

Die Grenzen der  
Chemie neu ausloten?  
It takes  
#HumanChemistry

Wir suchen kreative Chemikerinnen und Chemiker,  
die mit uns gemeinsam neue Wege gehen wollen –  
mit Fachwissen, Unternehmertum und Kreativität für  
innovative Lösungen. Informieren Sie sich unter:

[evonik.de/karriere](https://evonik.de/karriere)

# Generalized Analysis Approach of the Profile Roughness by Electron Microscopy with the Example of Hierarchically Grown Polystyrene–Iron Oxide–Silica Core–Shell–Shell Particles

Deniz Hülagü,\* Charlie Tobias, Estela Climent, Ardian Gojani, Knut Rurack,\* and Vasile-Dan Hodoroaba

The roughness as a property of core–shell (CS) microparticles plays a key role in their functionality. Quantitative evaluation of the roughness of CS microparticles is, however, a challenging task with approaches using electron microscopy images being scarce and showing pronounced differences in terms of methodology and results. This work presents a generalized method for the reliable roughness determination of nonplanar specimens such as CS particles from electron microscopic images, the method being robust and reproducible with a high accuracy. It involves a self-written software package (Python) that analyzes the recorded images, extracts corresponding data, and calculates the roughness based on the deviation of the identified contour. Images of single particles are taken by a dual mode scanning electron microscopy (SEM) setup which permits imaging of the same field-of-view of the sample with high resolution and surface sensitive in SE InLens mode as well as in transmission mode (TSEM). Herein, a new type of polystyrene core–iron oxide shell–silica shell particles is developed to serve as a set of lower micrometer-sized study objects with different surface roughness; the analysis of their images by the semiautomatic workflow is demonstrating that the particles' profile roughness can be quantitatively obtained.

## 1. Introduction


Core–shell (CS) particles have gained an increasingly important role in a broad range of applications such as drug delivery and tissue engineering, catalysis and separation, imaging and sensing, environmental remediation and photovoltaics, and 3D printing and the food industry.<sup>[1–6]</sup> This popularity is due to the fact that the development of advanced CS particles has opened up plenty of opportunities for enhanced functionality and performance.<sup>[7,8]</sup> CS particles can be designed to show unique properties depending on the combination of their organic and inorganic constituent materials.<sup>[6]</sup> The properties of such particles can be primarily tailored by controlling their composition, size, core-to-shell ratio, or architectural hierarchy in multicore/single-shell or single-core/multishell systems.<sup>[9]</sup> Moreover, the methods for surface modification of such particles are abundant, potentiating the means to increase functionality to meet

diverse application requirements. In particular, micrometer-sized beads are well suited for the quantitative detection of analytes of interest by single particle-based (bio)analytical methods because of their rapid reaction kinetics and the requirement of small sample volumes, an area of application we became interested in over the past years.<sup>[10–14]</sup> A very promising material combination for single particle-based assays is achieved by merging the benefits of polystyrene (PS) and silica (SiO<sub>2</sub>) particles in a core–shell particle format.<sup>[12,15,16]</sup>

Besides equipping CS particles with optical or electrochemical features and grafting (bio)chemical units to their outer surface that drive many of the developments in the field, two less explicit aspects gained increasing attention recently, surface morphology and its impact on functional performance<sup>[10,17,18]</sup> as well as magnetic properties, strongly facilitating handling and processibility<sup>[19,20]</sup> especially in view of automated workflows.<sup>[21,22]</sup> Examples of CS particles with magnetic features and controlled surface morphology, however, are scarce.<sup>[23,24]</sup> In the current work, we report on the synthesis and in-depth

D. Hülagü, V.-D. Hodoroaba  
Division 6.1 Surface Analysis and Interfacial Chemistry  
Bundesanstalt für Materialforschung und -prüfung (BAM)  
Unter den Eichen 44-46, 12203 Berlin, Germany  
E-mail: deniz.huelague@bam.de

C. Tobias, E. Climent, A. Gojani, K. Rurack  
Division 1.9 Chemical and Optical Sensing  
Bundesanstalt für Materialforschung und -prüfung (BAM)  
Richard-Willstätter-Straße 11, 12489 Berlin, Germany  
E-mail: knut.rurack@bam.de

 The ORCID identification number(s) for the author(s) of this article can be found under <https://doi.org/10.1002/adem.202101344>.

© 2022 The Authors. Advanced Engineering Materials published by Wiley-VCH GmbH. This is an open access article under the terms of the Creative Commons Attribution License, which permits use, distribution and reproduction in any medium, provided the original work is properly cited.

DOI: 10.1002/adem.202101344

characterization of PS core–iron oxide shell–SiO<sub>2</sub> shell microparticles designed to be eventually used in an automated analyzer for the immunochemical detection of lead contaminants in point-of-need settings.<sup>[25]</sup> Because such particles require functionalization by decorating them with bioreceptors, not only is a reproducible particle synthesis procedure important but also is their characterization essential to establish a reliable and robust performance.<sup>[26]</sup> The roughness of a core–shell particle is especially important because the surface roughness affects the accessibility to any functional (bio)molecule grafted to it, in this case acting as binding units, thus influencing sensitivity in a (bio) analytical setting.<sup>[10]</sup>

Particle characterization involving the measurements of size, size distribution, shell thickness and surface texture, and surface area and morphology is commonly carried out with a canon of well-known analytical methods.<sup>[27,28]</sup> The most common technique used for size and particularly shape and detailed surface morphology analysis of particles is based on scanning electron microscopy (SEM).<sup>[29,30]</sup> In addition to particle size and shape, for CS particles the SEM images also reveal information on the homogeneity of the usually comparatively thin shell that covers the core particle. SEM is a relatively fast characterization technique compared with other high-resolution imaging methods because sample preparation and image acquisition procedures are well established, easily controlled, and readily performed. When SEM is equipped with an energy-dispersive X-ray spectrometer (EDS), qualitative elemental analysis of the core–shell structure can be conducted.<sup>[31]</sup> Transmission electron microscopy (TEM) provides mostly more information on overall particle size or uniformity of the shell due to the superior spatial resolution of the technique.<sup>[32]</sup>

Roughness has been extensively used as a parameter for surface characterization when employing atomic force microscopy (AFM).<sup>[33–36]</sup> In contrast, the literature that addresses this issue for nonplanar particles using SEM or TEM imaging is scarce and only qualitative.<sup>[37,38]</sup> Moreover, reported research in the literature on roughness analysis shows large differences in terms of methodology and reported results.<sup>[39,40]</sup> The literature lacks a systematic, quantitative evaluation of the roughness of single core–shell particles where the shell morphology is of great interest. Therefore, development of a generalized method for reliable roughness determination of strongly curved surfaces of such core–shell particles with a diameter in the micrometer range from microscopic images is required. This can serve as a validation for AFM measurements and as an alternative measurement method which is simpler and faster to perform compared with the existing ones.

The quantification of the surface roughness of a microbead-type particle can be done in different ways, but the most common method is by using the root mean square (RMS) amplitude from the height of the mean level along a defined profile over the particle surface.<sup>[41]</sup> In other words, root mean squared profile roughness (RMS-R<sub>Q</sub>) is quantified as the variation of the fine deviations from an ideal shape of the particle in a localized domain, as opposed to the coarse deviations which would result from the deviation of the overall shape of the particle. An alternative parameter for roughness quantification is the peak-to-valley height, which corresponds to maximum height difference

and is applicable in the cases where the density of fine deviations is very small.<sup>[42]</sup>

To our knowledge, no fully automated procedure exists in the literature for the quantitative evaluation of a bead's roughness using electron microscopy (EM) images. EM images are commonly analyzed visually depending on the operator's interpretation and classified into rough or smooth. This work thus systematically focuses on fundamental image analysis steps to provide a reliable tool to calculate a particle's profile roughness with high accuracy and reproducibility, as a robust and semiautomatic procedure from EM images. The ideal shape of the particles is assumed spherical; hence, its parallel projection onto the image plane is a circle. Our image analysis tool involves a self-written software package which analyzes the recorded EM images (of both types, SEM and transmission mode SEM or TSEM). The proposed software extracts corresponding data and calculates the roughness based on the deviation of the recorded circumference (contour) from a circular one. Previously, a particle roughness analysis tool, based on EM images, was reported by Sarma et al.<sup>[26]</sup> In the present work, a new Python script was developed to evaluate quantitatively EM images with respect to their surface roughness. The new script provides high accuracy and reproducibility because as many as possible analysis steps were automatized. The image analysis tool we developed was designed more systematically compared to the previous one by evaluating extensive variation of some parameters, such as threshold value and accelerating voltage. Moreover, the image analysis tool can also be used for boundary detection and roughness analysis of particles of any shape. The software code used in this work for image analysis is freely available on the GitHub repository *Roughness-Analysis-by-Electron-Microscopy*.<sup>[43]</sup>

The main challenges associated with image processing are also addressed in this work. Probably the most critical step in the image analysis sequence is the binarization by setting an appropriate threshold value to the grayscale EM images, which results in a segmentation to outline the particle boundaries. Segmentation is generally described as separating an image into various areas in which pixels have similar grayscale values.<sup>[44]</sup> Thresholding-based segmentation is one of the most popular techniques that is adaptable in the analysis of EM images.<sup>[26]</sup> As the entire subsequent analysis steps strongly rely on the segmentation results, the most demanding task is to find the proper threshold value. Thus, the most significant source of measurement uncertainties shall be attributed to the setting of the true threshold value.

## 2. Results and Discussion

The microparticles of this work present a functional advancement of the PS core–silica shell microbead platform recently introduced by us<sup>[10,26]</sup> in the sense that they incorporate a first magnetic iron oxide shell and a second, outer silica shell, which shields the polymer core (e.g., against dissolution when working with organic (co-)solvents), confines and separates the magnetic layer (e.g., avoiding a negative influence on functional entities such as fluorescent or redox-active species attached to the outer particle surface), and allows for facile roughness tuning. A set of particles with various degrees of roughness was thus produced

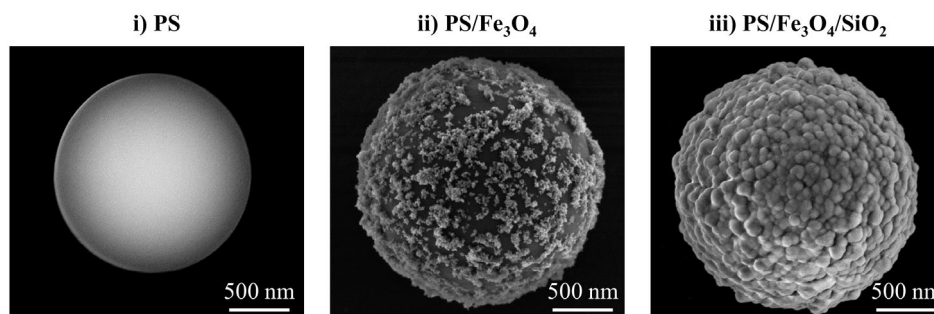


**Figure 1.** SEM images of a representative particle of the set of particles produced along the synthesis workflow, differing in roughness: i) PS core particle with  $d_{\text{mean}} = 1.8 \mu\text{m}$ , ii) PS/Fe<sub>3</sub>O<sub>4</sub> core-shell particle, iii) PS/Fe<sub>3</sub>O<sub>4</sub>/SiO<sub>2</sub> core-shell-shell particle with an overall shell thickness of  $\approx 75 \pm 17 \text{ nm}$ .

along the synthesis workflow from core via core-shell to core-shell-shell particles (Figure 1). Highly monodisperse PS core particles of an average diameter of  $d_{\text{mean}} = 1.8 \mu\text{m}$  were synthesized according to an established protocol and served as a reference sample that represents the smoothest surface condition. Although there were differences in diameter of up to 200 nm between different synthesized batches of PS particles, these variations of the smooth core particles had no influence on the formation of the shell or its final roughness. These PS cores were covered with a layer of superparamagnetic iron oxide (Fe<sub>3</sub>O<sub>4</sub>) nanoparticles with an average size of  $d_{\text{mean}} = 7 \pm 1 \text{ nm}$  (Figure S4b, Supporting Information), resulting in PS/Fe<sub>3</sub>O<sub>4</sub> core-shell particles. By design, this first layer is not a dense one, as the aim was to introduce the magnetic function without completely shielding the PS core so that in future work the core can be optically encoded which is important for (bio)analytical methods relying on multiplexing through encoded microparticles.<sup>[11,12]</sup> For the final core-shell-shell particles, these PS/Fe<sub>3</sub>O<sub>4</sub> particles were covered with a thin protective silica (SiO<sub>2</sub>) shell, yielding PS/Fe<sub>3</sub>O<sub>4</sub>/SiO<sub>2</sub> beads. As mentioned above, the latter is primarily important to be able to fully exploit the functionalization chemistry of silica surfaces without leading to unwanted chemical reactions with the polymeric core material. The average thickness of the two shells was determined to be  $75 \pm 17 \text{ nm}$  from TEM images, as presented in Figure S6c, Supporting Information.

Further details on the particles' scattering properties, their primary chemical functionalization and surface charges as well as their chemical composition and features of the Fe<sub>3</sub>O<sub>4</sub> nanoparticles are given in the Supporting Information.

In view of the rational design of functional particles, a key step would be to connect morphological features which can be synthetically controlled (as illustrated in Figure 1) to final performance parameters. While characterization methods of the bulk as well as the surface chemistry of CS particles are well-established, their link, the morphological characteristics, are usually only phenomenologically described so that we developed here an image processing procedure to reliably evaluate the profile roughness of a single microparticle with high accuracy by analyzing its contour in a standardized manner. Our approach involves segmentation of the recorded EM images (SEM and TSEM) of the single particles and an automated data extraction software to evaluate profile roughness from the segmented

images. An emphasis was particularly put on the quality of the image segmentation to find the true threshold value. Special focus was also laid on the investigation of the influence of the accelerating voltage (extra-high tension [EHT]) on the calculated profile roughness.

## 2.1. The Image Processing Workflow

The image processing workflow developed in this work involves five steps. An exemplary illustration is depicted in Figure 2 for an SEM image of a single particle. The same procedure is applied to the TSEM images.

### 2.1.1. Measurement

Images of single particles were taken with an SEM instrument which enables transmission electron microscopy mode (TSEM) as well. A small working distance ( $\text{WD} = 2.8 \text{ mm}$ ) was used. For the imaging with both SEM and TSEM modes, no coating of the sample was necessary.

### 2.1.2. Threshold

The elements of the SEM image matrix are grayscale values of the intensity proportional to the number of secondary electrons (SEs) (in case of TSEM, transmitted electrons) emitted by the material surface being imaged. Thus, the variation of pixel grayscale values in an SEM micrograph reveals the shape and the morphology of the particle. To extract roughness data from an EM image the next task is segmentation, in other words to convert the initial image into a binary image. In this way, pixels of the image can be classified as being a part of the foreground or the background. As a result, the object of interest can certainly be identified. The selection of the threshold algorithm is discussed in Section S1.1, Supporting Information. Depending on these results, an automated threshold based on IsoData algorithm was applied to the image with the Gwyddion software to obtain a binary image. Besides Gwyddion is a freely available software developed for scanning probe microscopy (SPM), it is also used for grayscale image processing (<http://gwyddion.net/>). The gross errors such as visible voids, which might affect the accuracy of the image segmentation, were manually corrected. Such corrections and also automated thresholding will be implemented into

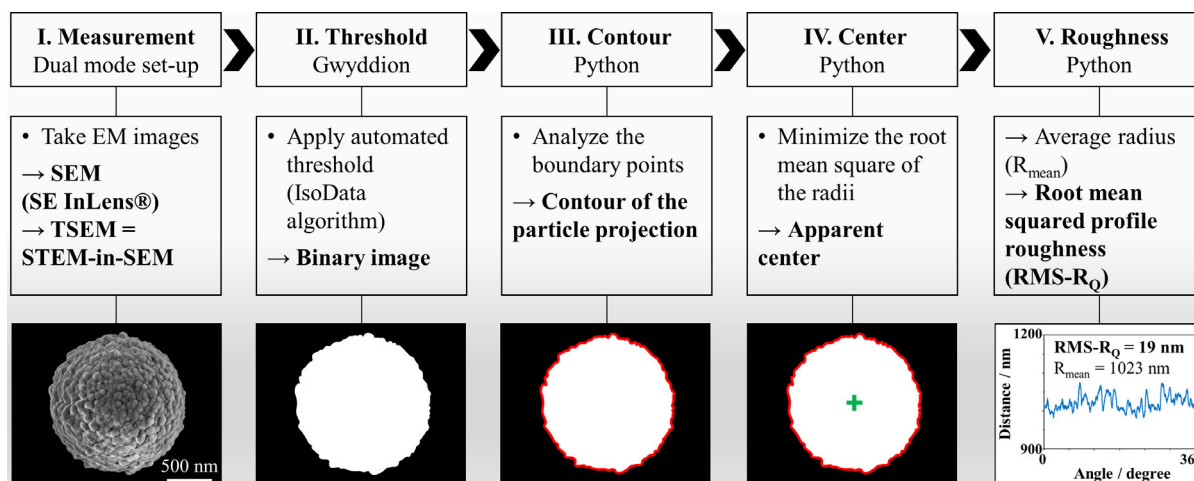


**Figure 2.** Flowchart of the processing sequence of a SEM/InLens micrograph with the proposed image analysis approach.

the code with the final goal of a complete automated image processing workflow.

### 2.1.3. Contour

The following steps are carried out by the developed Python script. The script scans over each pixel (1 pixel = 1.84 nm) of the binary image and identifies all possible boundary points when the pixel changes from black to white, or vice versa (Figure 3a). When a pixel is detected as one of the boundary

points ( $p_b$ ), its 8-neighbor pixels ( $p_n$ ) are also scanned (Figure 3b). If there is at least one pixel in the neighborhood with the opposite value, the detected point is confirmed as an identified boundary point ( $p_{(x,y)}$ ). Neighborhood scanning eliminates the regions which are not connected to the boundary of the particle (Figure 3c). Hence, in this way the complete contour of the particle is identified (red line in Figure 3d).

### 2.1.4. Center

The average of the identified boundary points (see the red plus mark in Figure 4a) gives the initial center point of the particle. The distances ( $d_i$ ) between this initial center and each identified boundary point are calculated (Figure 4b). The self-written script adjusts the calculated center point in  $\pm\Delta x$  and  $\pm\Delta y$  directions with an iteration and calculates each time the standard deviation of the distances. The iteration continues with standard deviation of the distances decreasing and stops when the minimum standard deviation of the distances is reached (Figure 4c); consequently, the apparent center of the particle projection is estimated (green plus mark in Figure 4d).

### 2.1.5. Roughness

The calculated distances from previous step correspond to the radii ( $d_r$ ). Then, the RMS- $R_Q$  of the particle projection is calculated (Figure 4e) as the standard deviation of the radii by Equation (1) as follows

$$\text{RMS-}R_Q = \sqrt{\frac{1}{N} \sum_{i=0}^N d_r^2} \quad (1)$$

where  $N$  is the number of pixels that define the contour. When the radii are plotted against the respective angle, the lateral profile is also obtained as presented in Figure 4e (green line in the graph).

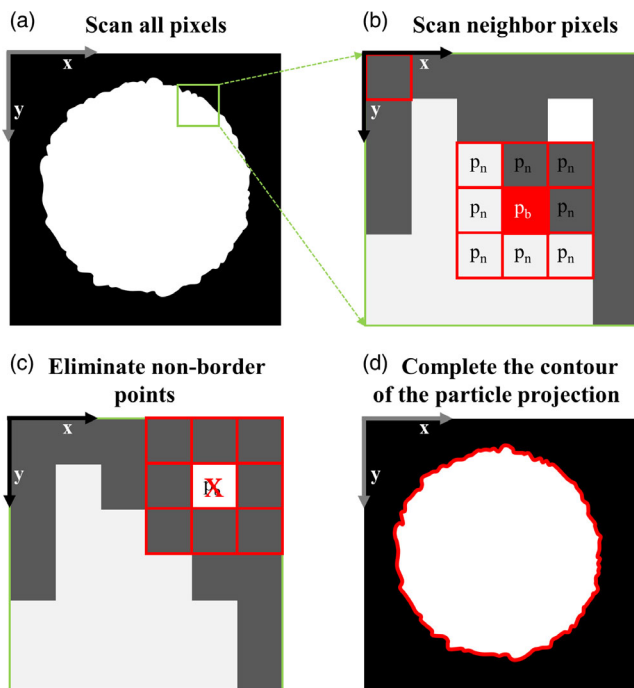


**Figure 3.** Illustration of the procedure for identification of the contour of the particle (red line in d) with the proposed image analysis approach.

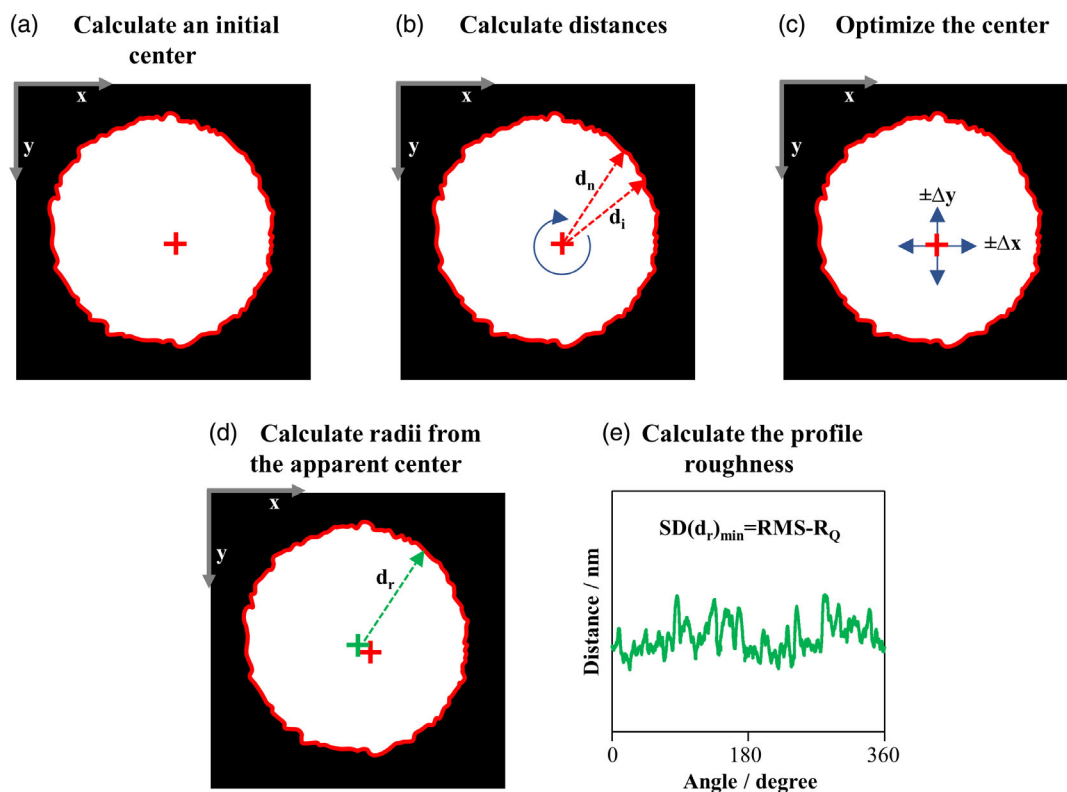


**Figure 4.** Illustration of the procedure for finding the center of the particle and calculating the roughness with the proposed image analysis approach.

## 2.2. Finding the Threshold Value

As previously mentioned, the threshold value considerably affects the boundary position. Consequently, the overall size and especially the roughness of the extracted object are changed. As the subsequent image analysis steps are sensitive to the selected threshold value, the establishment of the proper threshold value, that is the threshold value, which is subsequently used for image binarization, is of crucial importance.

**Figure 5** presents an example of grayscale value histograms of a pair of SEM and TSEM images of the same single PS/Fe<sub>3</sub>O<sub>4</sub>/SiO<sub>2</sub> particle recorded at 5 kV with the dual mode SEM setup. The SEM image was binarized with the IsoData algorithm (by Gwydion software) at three different threshold values of 8%, 15%, and 20%. The threshold values were selected within the range between the two peaks of the histogram. Binarized images by threshold were analyzed by the developed Python roughness analysis tool.

SEM images spread a large range along the entire grayscale values and offer narrower range of threshold values that can be applied. This makes the binarization of the SEM images very sensitive to the applied threshold value. Results show that the contour of the particle was accurately identified when the threshold value was set to 8%. However, when the threshold value was increased from 8% to 20%, features on the boundary of the particle projection became invisible, the continuity of the contour was disrupted, and gaps were formed. As a result, more pixels were misleadingly identified as boundary points. This means that

at higher threshold values part of the information was lost. Accordingly, the profile roughness of the particle is underestimated at higher threshold values. Root mean squared roughness of the particle within the selected threshold range decreased from 25 to 19 nm, which corresponds to a significant change of 24%.

The same thresholding procedure was applied to the equivalent TSEM image. Unlike the SEM, in case of TSEM the possibility for threshold selection from a wider range without significant effect on the image enables an easier identification of the particle contour. In TSEM case, 8%, 15%, and 45% threshold values were set to obtain corresponding binarized images for the further steps of image analysis. Contrary to the case of SEM images, TSEM images provide better mass thickness contrast, and hence, better defined particle boundaries, which makes the thresholding not only easier, but also more accurate, compared to SEM images. Increasing the threshold value from 8% to 20% for the TSEM image does not change significantly the obtained binarized image, as expected. Even though more boundary points were identified at lower threshold values, the calculated profile roughness stayed almost constant at 20 nm. The average radius ( $R_{\text{mean}}$ ) of the particle was also calculated as a side-result of the software program.

SEM- and TSEM-based roughness of the same single particle of PS/Fe<sub>3</sub>O<sub>4</sub>/SiO<sub>2</sub> is plotted in **Figure 6** as a function of the threshold value. Images were recorded at 2, 5, 10, and 15 kV, and then binarized. For TSEM, a slight alteration of the roughness was observed for thresholds smaller than 15%. For SEM, increasing the threshold value up to 10% did not change the

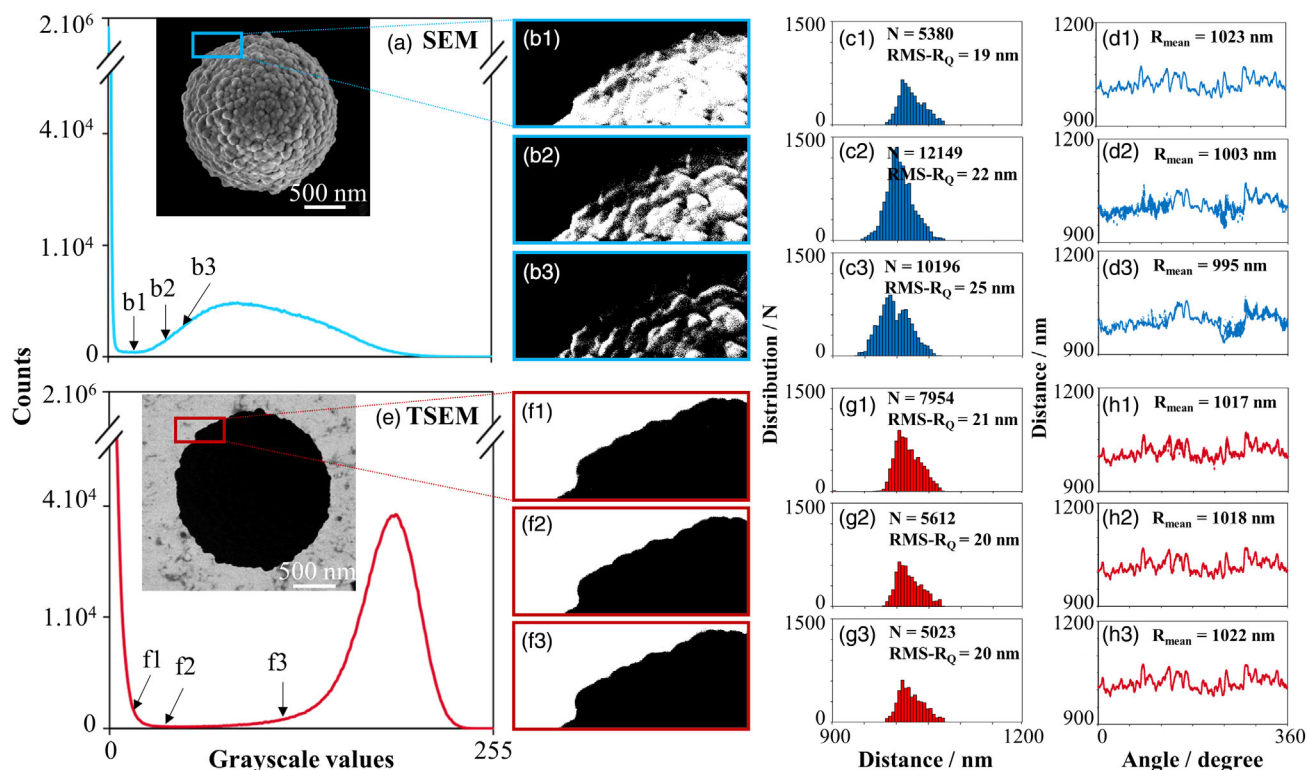


**Figure 5.** Grayscale histogram of a) SEM and e) the corresponding TSEM image of a single PS/Fe<sub>3</sub>O<sub>4</sub>/SiO<sub>2</sub> particle recorded at 5 kV with the dual mode SEM setup. Thresholding the SEM image with the IsoData algorithm at values of b1) 8%, b2) 15%, and b3) 20%. c1–c3) Calculated distribution of distances and d1, d2, d3) the lateral profile as a function of angle for the respective binarized images. Thresholding the TSEM image with the IsoData algorithm at values of f1) 8%, f2) 15%, and f3) 45%. g1–g3) Calculated distribution of distances and h1–h3) the lateral particle profile as a function of angle for the respective binarized images ( $N$  = number of identified border points,  $RMS-R_Q$  = root mean squared profile roughness,  $R_{mean}$  = average radius).

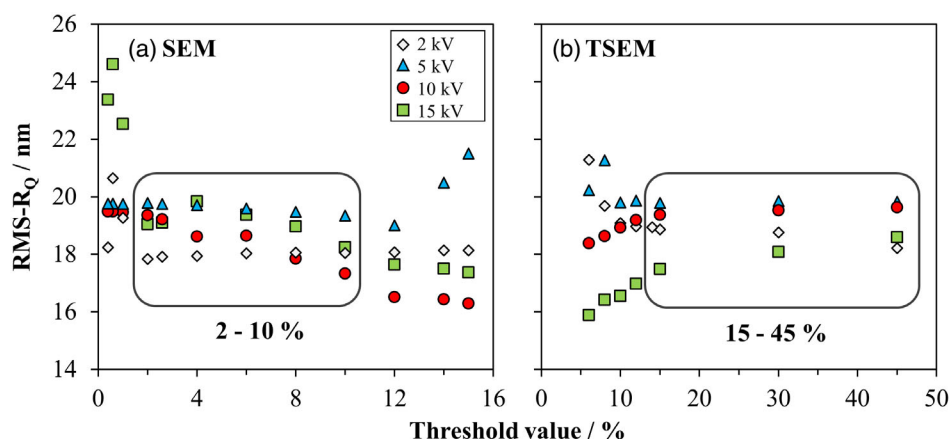


**Figure 6.** Selection of threshold value for a) SEM and b) TSEM images. Thresholding was applied with the IsoData algorithm by Gwydion software. The framed regions mark those threshold values for which the roughness remains unchanged.

outcome. At values higher than 10%, a strong variation of the threshold value was observed. Calculations were repeated for images recorded at different accelerating voltages. The results reveal that, for SEM images, threshold values between 2% and

10% yield the same roughness values and the approach constitutes, hence, a robust calculation. For TSEM, the suitable threshold range where the calculated roughness values do not show significant differences lies between 15% and 45%.

### 2.3. Influence of Accelerating Voltage

Only few studies have been reported in the literature on the influence of accelerating voltage, called EHT, on the measurement of nanoparticles.<sup>[45]</sup> Acquisition of SEM images at higher accelerating voltages provides higher resolution. In SEM, lower accelerating voltages result in more surface-sensitive images but worse resolution. Dependency on EHT can also be considered as another source of measurements uncertainty. Therefore, the influence of the accelerating voltage on the calculated profile roughness must be evaluated and the robustness of the proposed image analysis approach needs to be verified.

For this investigation, images of the same particle were acquired at various EHTs between 2 and 15 kV with both modes, SEM and TSEM. All other measurement parameters, such as scan speed, magnification, or pixel size, were kept identical. Each image was binarized at three different threshold values within the suitable range as set in Figure 6. The roughness values of these three images were calculated and the average value was plotted against EHT for each microscopy mode (Figure 7a,b).

Based on SEM images, the PS/Fe<sub>3</sub>O<sub>4</sub>/SiO<sub>2</sub> particle showed the highest profile roughness from the set of three selected types of particles. The profile roughness of a PS/Fe<sub>3</sub>O<sub>4</sub> particle was slightly lower than that of PS/Fe<sub>3</sub>O<sub>4</sub>/SiO<sub>2</sub>, and as expected, a PS particle revealed the smoothest profile. The same trend was visible for the TSEM-based calculations. Both TSEM- and SEM-based profile roughness values show no change on EHT within the set range, except for the SEM-based roughness of the PS/Fe<sub>3</sub>O<sub>4</sub> particle. The SEM-based calculated roughness values of that sample showed a slight tendency to increase with an increase in accelerating voltage. Based on the available series of data this minor trend cannot be attributed to a clear effect. For the other type of particles, no alteration was observed for both SEM- and TSEM-based analysis within the set EHT range. Moreover, both SEM- and TSEM-based analyses resulted practically in the same roughness.

As an independency of EHT was observed, the profile roughness of a particle can also be presented as the average of the overall data obtained from the images recorded at different EHTs (Table 1) as plotted in Figure 7c. This diagram clearly

**Table 1.** SEM- and TSEM-based RMS-R<sub>Q</sub> values calculated with the proposed image analysis toll.

Particle	SEM-based RMS-R <sub>Q</sub> [nm]	TSEM-based RMS-R <sub>Q</sub> [nm]
i) PS	4 ± 1	4 ± 0
ii) PS/Fe <sub>3</sub> O <sub>4</sub>	17 ± 3	15 ± 2
iii) PS/Fe <sub>3</sub> O <sub>4</sub> /SiO <sub>2</sub>	19 ± 1	19 ± 1

shows three well-defined categories of particles with various roughness values, which means that our particle analysis procedure is convenient to distinguish profile roughness quantitatively. These results also evidenced that SEM- and TSEM-based roughness values of PS and PS/Fe<sub>3</sub>O<sub>4</sub>/SiO<sub>2</sub> particles are in excellent agreement. This good matching indicates that the proposed method of determining the particle profile roughness is accurate, and not affected by method bias. Moreover, flow cytometry provides particle sizes as complementary data to the roughness values derived by the present image analysis procedure, flow cytometry being another independent single particle characterization technique. The data measured by flow cytometry are presented in the Supporting Information.

It should be noted here that depending on the used materials, the TSEM mode provides important information on shell formation with contrast difference between shell and background, which makes it easier to identify boundary points. More valuable insight into the shell fine structure is given with SEM mode with its superior surface morphological contrast.<sup>[1,46]</sup>

### 3. Conclusion and Outlook

This work constitutes a further development of the study initiated by Sarma et al.<sup>[26]</sup> on determining the roughness of spherical microparticles from the projected contour using EM images. This extension included a newly developed particle format by inserting a layer of iron oxide nanoparticles between the PS core and the silica shell of our earlier system, arriving at a core-shell-shell platform with additional magnetic properties and providing a set of three different particle types with varying surface

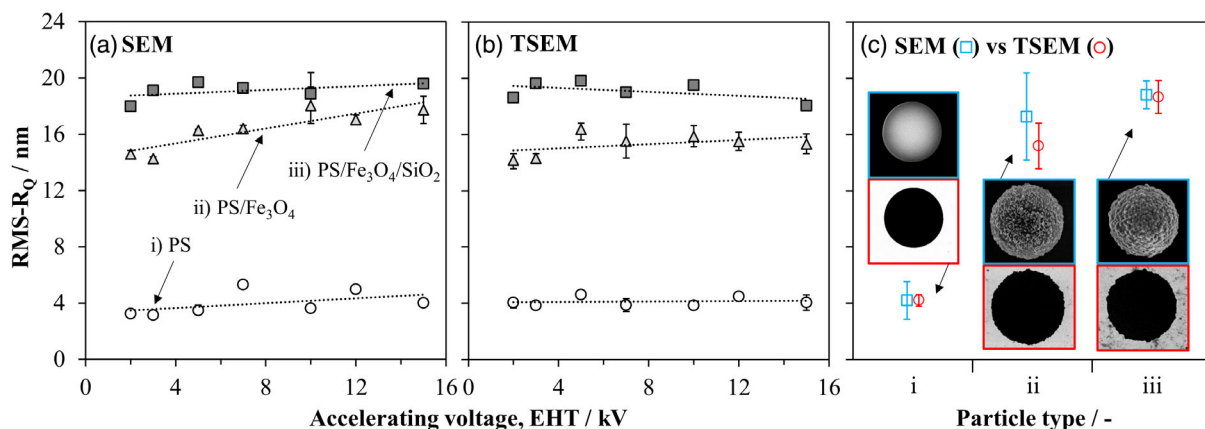


**Figure 7.** Influence of accelerating voltage on the calculated particle profile roughness from a) SEM images and b) TSEM images. (c) Compares the average of profile roughness at all accelerating voltages as calculated from SEM and TSEM images for the three different types of particles (see Table 1).



morphology, ideally suited to test our new analysis approach. Within the latter, the application of a threshold value for image binarization and segmentation, such that the contour is automatically determined, must be carefully estimated. Compared to SEM, TSEM images were more robust with respect to the variation of threshold values, due to the higher mass thickness contrast underlying this type of imaging. In any case, the automatic thresholding using the IsoData procedure segmented the image into background and foreground by setting the threshold value at 8% of the pixel intensities. After the extraction of the particle contour, the roughness was calculated as the RMS deviation from the overall radius of the particle, which was also determined in a parallel software routine.

The developed automatic image processing and analysis give robust quantitative determination of particle profile roughness; hence, particle characterization of other types of particles is possible. This result will assist to determine particle surface functionalization, and a concrete application is the decoration of particles with antibodies for use in immunosensors.

Our software analyzes one image (either SEM or TSEM), quantifies the profile roughness, and yields information about the size of an individual microparticle within a few seconds. This approach can further be used to analyze several single particles in a batch to evaluate the homogeneity or determine the change in roughness from batch to batch, if images are recorded with identical field of view, also independently of the image resolution.

In ongoing work, Monte Carlo simulations to understand better the SEM and TSEM signals for the investigated particles and a comprehensive assessment of the role of surface morphology on the performance of functional particles in a certain application are being addressed.

## 4. Experimental Section

**Materials:** Poly(vinylpyrrolidone) (PVP10 with an average molecular weight of 10 kD, Sigma), styrene (ReagentPlus, <99%, Sigma), basic alumina ( $\text{Al}_2\text{O}_3$ , Brockmann I, Acros), and azo-bis-cyanovaleic acid (ACVA, MP Biomedicals) were used for the PVP-coated PS core synthesis. Tetraethoxyorthosilicate (TEOS, <99%, Merck) was used for the silica coating. (3-Aminopropyl)triethoxysilane (APTES, 99%, Aldrich) was used for amino-functionalization. Ethanol (abs. 99% and 96%, ChemSolute) and water of MilliQ grade (BAM) were used as solvents and for washing.

**Particle Synthesis—PS Core Synthesis:** PS particles were synthesized by dispersion polymerization as previously reported by us.<sup>[13]</sup> The polymerization was carried out in a hybridization oven. A solution of 105 mg of ACVA in 10 mL methanol was prepared in an argon atmosphere. In glass vials, 170 mg PVP10 were dissolved in 10 mL ethanol, before adding 1 mL of styrene, previously filtered through basic aluminum oxide. The mixture was flushed with argon for 30 min. The reaction was started by adding 0.5 mL of the ACVA solution and then left stirring overnight at 70 °C under an argon atmosphere. Afterward, the particles were centrifuged, washed multiple times with water and ethanol, before drying at room temperature.

**Particle Synthesis—Coating of PS Cores with Iron Oxide Nanoparticles,  $\text{PS}/\text{Fe}_3\text{O}_4$ :** First, superparamagnetic iron oxide nanoparticles were synthesized. In a round bottom flask, 0.338 g of  $\text{FeCl}_3 \times 6 \text{H}_2\text{O}$  and 0.172 g  $\text{FeCl}_2 \times 4 \text{H}_2\text{O}$  were dissolved in 100 mL Milli-Q water. The solution was flushed with argon for 20 min before adding dropwise a solution of 4 g PVP10 in 58 mL  $\text{NH}_3$  solution (16%). The reaction was stirred for 1.5 h with a mechanical stirrer at 150 rpm. The particles were washed multiple times with water via magnetic separation and subsequently stored in a refrigerator in a concentration of  $\approx 3\%$  w/v in Milli-Q water.

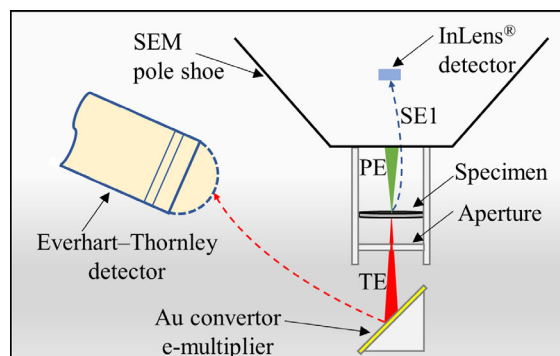


**Figure 8.** Sketch of dual SEM/TSEM setup. Adapted based on Hodoroaba et al.<sup>[46]</sup>

To coat the polymer cores with a superparamagnetic nanoparticle layer, a solution of 60 mg PS and 2 mL  $\text{Fe}_3\text{O}_4$  particles ( $\approx 3\%$  in water) was prepared in 30 mL Milli-Q water in Falcon tubes. Coating was carried out after placing the tubes on a rotator plate at 40 rpm during 1.5 h. Afterward, the particles were washed twice with water and once with ethanol, before drying.

**Particle Synthesis—Coating of  $\text{PS}/\text{Fe}_3\text{O}_4$  Particles with Silica Shell,  $\text{PS}/\text{Fe}_3\text{O}_4/\text{SiO}_2$ :** First, 60 mg of  $\text{PS}/\text{Fe}_3\text{O}_4$  particles were dispersed in 30 mL ethanol and 1 mL Milli-Q water. Then, while stirring with a mechanical stirrer at 150 rpm, 555  $\mu\text{L}$   $\text{NH}_3$  solution (32%) was added, followed by the dropwise addition of 555  $\mu\text{L}$  TEOS. The mixture was stirred overnight at 38 °C, and then washed with water and ethanol multiple times and dried at room temperature.

**Instrumentation and Image Acquisition:** The particles were suspended in ethanol and ultrasonication was applied for 5 min. The samples for analysis were prepared by drop-casting on conventional carbon TEM grids. Images of individual particles were recorded with a Scanning Electron Microscope of type Zeiss Supra 40 (Zeiss, Oberkochen, Germany) equipped with a high-resolution cathode (Schottky field emitter), an Everhart–Thornley SE detector and an SE InLens detector (Figure 8).<sup>[46]</sup> For the transmission electron microscopy mode (TSEM, or STEM-in-SEM), a dedicated “transmission” sample holder has been used. Details on its construction, operation, and performance are presented elsewhere.<sup>[46]</sup> The samples on the thin film TEM grid are placed on the sample holder. The transmission setup involves a gold converter as a multiplier of the transmitted electrons, which was then mounted on the SEM stage for analysis. This instrumental configuration offers several practical advantages. The observation of the sample surface from the top is performed by SEM mode with an InLens detector. The screening ring plays an essential role for the TSEM mode by blocking the SEs toward the Everhart–Thornley detector.

## Supporting Information

Supporting Information is available from the Wiley Online Library or from the author.

## Acknowledgements

D.H. and C.T. contributed equally to this work. This work has been performed as a part of the BAM Focus Area Project “MamaLoCA—Modular, multiplexed, antibody-based lab-on-chip analyzer for food control,” for which financial support by BAM is acknowledged (TF20). The authors are grateful to S. Benemann (Surface Analysis and Interfacial Chemistry Div., BAM) for SEM images, K. Gawlitza (Chemical and Optical Sensing Div., BAM) for TEM images, and A. Zimathies (Structural Analysis Div., BAM) for  $\text{N}_2$  adsorption/desorption measurements.

Open access funding enabled and organized by Projekt DEAL.

## Conflict of Interest

The authors declare no conflict of interest.

## Data Availability Statement

The data that support the findings of this study are available from the corresponding author upon reasonable request.

## Keywords

core-shell particles, image analysis, nanoparticles, roughness, scanning electron microscopy, transmission mode

Received: September 30, 2021

Revised: December 3, 2021

Published online:

- 
- [1] R. G. Chaudhuri, S. Paria, *Chem. Rev.* **2012**, *112*, 2373.
- [2] R. Hayes, A. Ahmed, T. Edge, H. F. Zhang, *J. Chromatogr. A* **2014**, *1357*, 36.
- [3] F. M. Galogahi, Y. Zhu, H. J. An, N. T. Nguyen, *J. Sci.: Adv. Mater. Devices* **2020**, *5*, 417.
- [4] R. Jenjob, T. Phakkeeree, D. Crespy, *Biomater. Sci.* **2020**, *8*, 2756.
- [5] H. Su, Q. Tian, C.-A. Hurd Price, L. Xu, K. Qian, J. Liu, *Nano Today* **2020**, *31*, 100834.
- [6] R. Singh, R. Bhatia, *Environ. Geochem. Health* **2021**, *43*, 2459.
- [7] S. Y. Wei, Q. Wang, J. H. Zhu, L. Y. Sun, H. F. Lin, Z. H. Guo, *Nanoscale* **2011**, *3*, 4474.
- [8] L. B. Wan, Z. L. Chen, C. X. Huang, X. T. Shen, *TrAC, Trends Anal. Chem.* **2017**, *95*, 110.
- [9] J. Wang, Q. Li, J. Xue, W. Chen, R. Zhang, D. Xing, *Chem. Eng. J.* **2021**, *410*, 127849.
- [10] D. Sarma, K. Gawlitza, K. Rurack, *Langmuir* **2016**, *32*, 3717.
- [11] D. Sarma, P. Carl, E. Climent, R. J. Schneider, K. Rurack, *ACS Appl. Mater. Interfaces* **2019**, *11*, 1321.
- [12] P. Carl, D. Sarma, B. J. R. Gregório, K. Hoffmann, A. Lehmann, K. Rurack, R. J. Schneider, *Anal. Chem.* **2019**, *91*, 12988.
- [13] C. Tobias, E. Climent, K. Gawlitza, K. Rurack, *ACS Appl. Mater. Interfaces* **2020**, *13*, 207.
- [14] E. Climent, R. Gotor, C. Tobias, J. Bell, P. M. Martin-Sanchez, K. Rurack, *ACS Sens.* **2021**, *6*, 27.
- [15] J. Y. Liu, J. Jarzabek, M. Roberts, D. Majonis, M. A. Winnik, *Langmuir* **2021**, *37*, 8240.
- [16] Y. Wang, C. Chen, J. He, Y. M. Cao, X. X. Fang, X. M. Chi, J. W. Yi, J. C. Wu, Q. S. Guo, H. Masoomi, C. Z. Wu, J. Ye, H. C. Gu, H. Xu, *Small* **2021**, *17*, 2100315.
- [17] S. Q. Liu, M. Y. Wei, P. Cool, C. Van Oers, J. Rao, *Microsc. Microanal.* **2011**, *17*, 766.
- [18] Z. A. Grady, A. Z. Arthur, C. J. Wohl, *Colloids Surf., A* **2019**, *560*, 136.
- [19] W. Liu, W. Zhong, Y. W. Du, *J. Nanosci. Nanotechnol.* **2008**, *8*, 2781.
- [20] Z. K. Sun, X. R. Zhou, W. Luo, Q. Yue, Y. Zhang, X. W. Cheng, W. Li, B. Kong, Y. H. Deng, D. Y. Zhao, *Nano Today* **2016**, *11*, 464.
- [21] Z. Chen, Y. Q. Wu, M. Kang, N. Y. He, S. R. Wan, E. B. Su, L. J. Wang, *Nanosci. Nanotechnol. Lett.* **2018**, *10*, 60.
- [22] W. Z. Yu, H. S. Lin, Y. L. Wang, X. He, N. Chen, K. Sun, D. Lo, B. Cheng, C. Yeung, J. W. Tan, D. Di Carlo, S. Emaminejad, *Sci. Rob.* **2020**, *5*, <https://doi.org/10.1126/scirobotics.aba4411>.
- [23] Q. Yue, Y. Zhang, Y. Jiang, J. Li, H. Zhang, C. Yu, A. A. Elzatahry, A. Alghamdi, Y. Deng, D. Zhao, *J. Am. Chem. Soc.* **2017**, *139*, 4954.
- [24] L. Yu, P. Pan, B. Yu, X. Yang, Q. Yue, A. A. Alghamdi, Y. Ren, Y. Deng, *ACS Appl. Mater. Interfaces* **2021**, *13*, 36138.
- [25] BAM Focus Area Project "MamaLoCA - Lab-on-Chip Analyser for food control", <https://www.bam.de/Content/EN/Projects/MamaLoCA/mamaloca.html>, (accessed: December 2021).
- [26] D. Sarma, J. Mielke, M. Sahre, U. Beck, V.-D. Hodoroaba, K. Rurack, *Appl. Surf. Sci.* **2017**, *426*, 446.
- [27] D. Su, *Green Energy Environ.* **2017**, *2*, 70.
- [28] M. M. Modena, B. Rühle, T. P. Burg, S. Wuttke, *Adv. Mater.* **2019**, *31*, 1901556.
- [29] A. E. Vladár, V.-D. Hodoroaba, in *Characterization of Nanoparticles*, (Eds: V.-D. Hodoroaba, W. E. S. Unger, A. G. Shard), Elsevier, Amsterdam **2020**, p. 7.
- [30] J. Yu, W. Liu, H. Yu, *Cryst. Growth Des.* **2008**, *8*, 930.
- [31] V.-D. Hodoroaba, in *Characterization of Nanoparticles*, (Eds: V.-D. Hodoroaba, W. E. S. Unger, A. G. Shard), Elsevier, Amsterdam **2020**, p. 397.
- [32] C. Chen, Z. Hu, Y. Li, L. Liu, H. Mori, Z. Wang, *Sci. Rep.* **2016**, *6*, 19545.
- [33] M. Hu, C.-P. Hsu, L. Isa, *Langmuir* **2020**, *36*, 11171.
- [34] A. San-Miguel, S. H. Behrens, *Langmuir* **2012**, *28*, 12038.
- [35] F. Sommer, T. M. Duc, R. Pirri, G. Meunier, C. Quet, *Langmuir* **1995**, *11*, 440.
- [36] X. Li, J. He, *ACS Appl. Mater. Interfaces* **2012**, *4*, 2204.
- [37] A. Schrade, V. Mailänder, S. Ritz, K. Landfester, U. Ziener, *Macromol. Biosci.* **2012**, *12*, 1459.
- [38] H. Zou, S. Wu, J. Shen, *Langmuir* **2008**, *24*, 10453.
- [39] G. Díaz, M. José-Yacamán, *Mater. Chem. Phys.* **1995**, *41*, 240.
- [40] L. Mammen, X. Deng, M. Untch, D. Vijayshankar, P. Papadopoulos, R. Berger, E. Riccardi, F. Leroy, D. Vollmer, *Langmuir* **2012**, *28*, 15005.
- [41] DIN ISO EN 25178-2:2012-09, DIN Deutsches Institut für Normung e.V., Berlin **2012**.
- [42] B. İlhan, C. Annink, D. V. Nguyen, F. Mugele, I. Siretanu, M. H. G. Duits, *Colloids Surf., A* **2019**, *560*, 50.
- [43] GitHub Repository for the Python Code, <https://github.com/BAMresearch/Roughness-Analysis-by-Electron-Microscopy>, **2021**, (accessed: December 2021).
- [44] C. Zheng, D. W. Sun, in *Computer Vision Technology for Food Quality Evaluation*, (Ed: D. W. Sun), Elsevier, San Diego, CA **2016**, 45.
- [45] L. Crouzier, A. Delvallée, S. Ducourtieux, L. Devoille, C. Tromas, N. Feltin, *Ultramicroscopy* **2019**, *207*, 112847.
- [46] V.-D. Hodoroaba, C. Motzkus, T. Macé, S. Vaslin-Reimann, *Microsc. Microanal.* **2014**, *20*, 1.